materials

MDPI

Article

First Principles Investigation of Binary Chromium Carbides Cr_7C_3, Cr_3C_2 and $Cr_{23}C_6$: Electronic Structures, Mechanical Properties and Thermodynamic Properties under Pressure

Liang Sun [1,2,*], Xiongshuai Ji [2], Liang Zhao [3], Wenyan Zhai [2,*], Liujie Xu [1], Hui Dong [2], Yanmin Liu [1] and Jianhong Peng [4]

1 National Joint Engineering Research Center for Abrasion Control and Molding of Metal Materials & Henan Key Laboratory of High-Temperature Structural and Functional Materials, Henan University of Science and Technology, Luoyang 471003, China; xlj@haust.edu.cn (L.X.); ymliu@xsyu.edu.cn (Y.L.)
2 Key Laboratory of Materials Processing Engineering, College of Materials Science and Engineering, Xi'an Shiyou University, Xi'an 710065, China; 19212050519@stumail.xsyu.edu.cn (X.J.); donghui@xsyu.edu.cn (H.D.)
3 Shaanxi Environmental Protection Group Ecological Construction Management Co., Ltd., Xi'an 710000, China; zeal228@163.com
4 School of Physics and Electronic Information Engineering, Qinghai University for Nationalities, Xining 810007, China; pjh@qhmu.edu.cn
* Correspondence: lsun@xsyu.edu.cn (L.S.); 180606@xsyu.edu.cn (W.Z.)

Abstract: Binary chromium carbides display excellent wear resistance, extreme stiffness and oxidation resistance under high temperature. The influence of applied pressure on electronic structure, elastic behavior, Debye temperature and hardness of Cr_7C_3, Cr_3C_2 and $Cr_{23}C_6$ have been investigated by the density functional theory (DFT) method. The results reveal that lattice parameters and formation enthalpy display an inverse relationship with applied pressure, and Cr_3C_2 exhibited optimal structural stability. Moreover, Cr-C orbital hybridization tends to be stronger due to the decreased partial density of states (PDOS) of the Cr atom. The difference in electronic distribution of binary carbides has also been investigated, which confirmed that overall orbital hybridization and covalent characteristics has been enhanced. The theoretical hardness was elevated according to the higher bond strength and bond density. In accordance with structural stability data, Cr_3C_2 has shown maximum theoretical hardness. Furthermore, the anisotropic nature of hardness has been evaluated with external pressure. Cr_3C_2, and the highest isotropic hardness behavior along with an increase in hardness values with increasing pressure has been observed. In addition, the variation in Debye temperatures of binary chromium carbides under applied pressure has also been predicted. The results provide a theoretical insight into electronic, mechanical and thermodynamic behavior of three binary chromium carbides and show the potential of these novel carbides in a wide range of applications.

Keywords: binary chromium carbides (Cr_7C_3; Cr_3C_2; $Cr_{23}C_6$); first-principles; electronic structure; elastic properties; hardness anisotropy; debye temperature

Citation: Sun, L.; Ji, X.; Zhao, L.; Zhai, W.; Xu, L.; Dong, H.; Liu, Y.; Peng, J. First Principles Investigation of Binary Chromium Carbides Cr_7C_3, Cr_3C_2 and $Cr_{23}C_6$: Electronic Structures, Mechanical Properties and Thermodynamic Properties under Pressure. *Materials* **2022**, *15*, 558. https://doi.org/10.3390/ma15020558

Academic Editor: Alexander A. Lebedev

Received: 18 November 2021
Accepted: 23 December 2021
Published: 12 January 2022

1. Introduction

Chromium carbide ceramics have exhibited great promise in a wide range of applications, such as cutting tool industry, fabrication of surface electrodes, and wear-resistant coatings. These materials can also be used as grain refinement agents in cemented carbide and other wear-resistance components due to their high melting point, good wear resistance, extreme stiffness and outstanding oxidation resistance under a high temperature environment [1,2]. As shown in the balanced Cr-C binary phase diagram, three stable structures of binary chromium carbides [2–11], including Cr_7C_3 (Pnma), Cr_3C_2 (Pnma) and $Cr_{23}C_6$ (Fm-3m) can be found at ambient temperature and atmospheric pressure, which have been extensively researched by several groups [2–18].

Cr_3C_2 has already been widely studied and used for industrial applications, due to its excellent mechanical and thermodynamic properties [8–15]. For instance, Cintho et al. [5] have fabricated high-purity Cr_7C_3 and Cr_3C_2 powders by using a high-energy ball-mill, followed by heat treatment at 800 °C for two hours. Zhang et al. [14] have observed that the thicker layer of Cr_3C_2 in electronic packing results in fine particles and improves its mechanical properties. Hirota et al. [12], Esteve et al. [13] and Hussainova et al. [15] have studied the mechanical properties of Cr_7C_3, Cr_3C_2 and $Cr_{23}C_6$ phases and reported Vicker hardness (H_v) values in the range of H_v (Cr_7C_3) = 5.71–17.0 GPa [12], 12.7–15.0 GPa [13], 21.0–22.0 GPa [15]. H_v (Cr_3C_2) = 15.1–18.9 GPa [12], 20–22 GPa [13], 17.4–18.5 GPa [15]; H_v ($Cr_{23}C_6$) = 12.7–15.0 GPa [12]. It is worth noting that the hardness values reported by different research groups are quite different due to the large variation in sample preparation methods and measurement protocols. Furthermore, several mechanical and electronic properties of these compounds cannot be experimentally measured due to certain experimental limitations, which highlights the significance and utilization of computational studies. On the theoretical front, Music et al. [7] have investigated the electronic structure and mechanical properties of orthogonal Cr_7C_3 based on first-principles and found that Cr-C bonds immerse in a large number of free electrons as the atomic chain of Cr-C-Cr, signifying the covalent bonding in orthogonal Cr_7C_3. Jiang et al. [9] have studied the phase structure, elastic behavior and electronic structure of different chromium carbides, and predicted the elastic modulus of these compounds for the first time. However, given the importance of high-pressure applications, such as aeronautics and astronautics, the performance of binary chromium carbides under pressure has not yet been explored.

Herein, we have employed first-principles calculations on the lattice parameters, electronic structure, elastic modulus and thermodynamic properties of binary chromium carbides under pressure, ranging from 0 to 10 GPa. The changes in electronic structure and mechanical properties, such as theoretical hardness, hardness anisotropy, and thermodynamic properties of Cr_7C_3, Cr_3C_2 and $Cr_{23}C_6$ under external pressure have been predicted. The present study provides a theoretical base for future experimental research and exhibits the promise of chromium carbide ceramics in a wide range of applications.

2. Calculation Methods and Models

All calculations on Cr_7C_3, Cr_3C_2 and $Cr_{23}C_6$ phases were performed by using the Cambridge Serial Total Energy Package (CASTEP) in Material Studio based on density functional theory (DFT) [19]. The Perdew-Burke-Ernzerhof (PBE) version of the generalized gradient approximation (GGA) was used to solve the equation of Kohn-Sham [20]. The ultra-soft pseudopotential method [21] was adopted to describe the interaction between valence electron and ion core [21], and the valence electrons for Cr and C atoms were $3s^2\ 3p^2\ 3d^5\ 4s^1$ and $2s^2\ 2p^2$, respectively. Based on the principle of minimum energy, all calculations were carried out in an inverted space and the cutoff energy of the plane wave was set to 350 eV. The number of *k*-points in the grid was in the Brillouin zone and *k*-points separation with the Monkhorst-Pack scheme for Cr_7C_3, Cr_3C_2 and $Cr_{23}C_6$ was $6 \times 4 \times 2$, $6 \times 10 \times 2$ and $2 \times 2 \times 2$, respectively [22]. The Broyden-Fletcher-Goldfarb-Shannon (BFGS) algorithm was applied to relax the whole structure and attain a ground state where both cell parameters and fractional coordinates of atoms are optimized simultaneously. The conditions of geometric optimization are as follows: the convergence precision of total energy is 1×10^{-6} eV/atom and the average force of each atom is within 0.002 eV/nm. The elastic constants were calculated by analyzing the changes in stress values resulting from the change in strain, i.e., stress–strain approach. The Parrinello-Rahman constant pressure method was used to change the pressure by adjusting the stress of primitive cell or primary cell, which affords shear force. The crystal structure of Cr_7C_3, Cr_3C_2 and $Cr_{23}C_6$ is shown in Figure 1. The pink-colored and blue-colored atoms represent Cr and C elements, respectively.

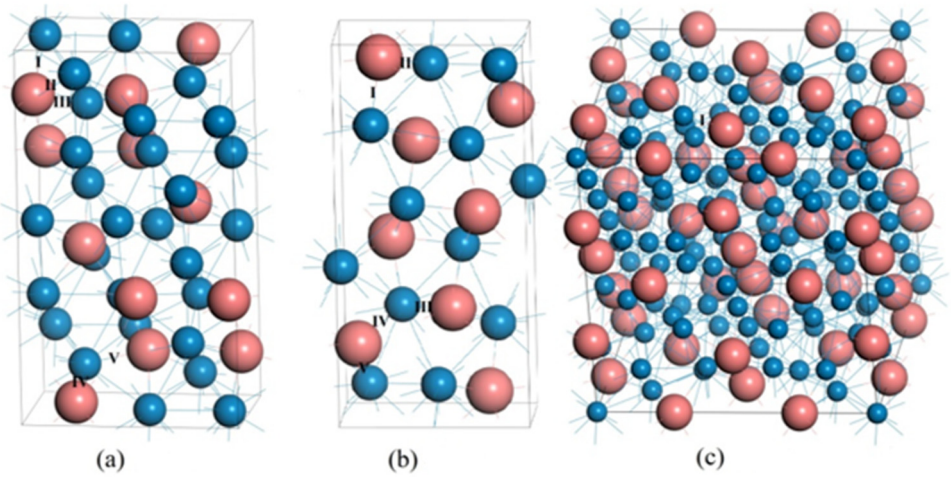

Figure 1. The crystal structure of (**a**) Cr_7C_3, (**b**) Cr_3C_2 and (**c**) $Cr_{23}C_6$.

3. Results

3.1. Lattice Parameters

The optimized structural parameters of Cr_7C_3, Cr_3C_2 and $Cr_{23}C_6$ phases are given in Table 1. Moreover, previous experimental results and theoretical calculations are included for comparison. For all binary Cr-C phases, the calculated lattice constants are consistent with the previous experimental and theoretical studies, implying that the employed pseudopotentials are reliable.

Table 1. Calculated parameters, formation enthalpy (ΔH), and DOS at the Fermi lever D_f of Cr_7C_3, Cr_3C_2 and $Cr_{23}C_6$ at zero pressure.

Compounds	Lattice Parameters (Å)			$-2\Delta H$/ (eV·Atom)$^{-1}$	D_f/ State (eV·Atom)$^{-1}$
	a	*b*	*c*		
Cr_7C_3	4.45 (4.51 [a], 4.53 [c])	6.84 (6.90 [a], 7.01 [c])	11.97 (12.08 [a], 12.14 [c])	0.183 (0.112 [a], 0.149 [b])	0.42 (0.43 [a])
Cr_3C_2	5.48 (5.49 [a], 5.54 [d])	2.79 (2.79 [a], 2.83 [d])	11.47 (11.47 [a], 11.49 [d])	0.157 (0.15 [b], 0.114 [a])	0.36 (0.36 [a])
$Cr_{23}C_6$	10.55 (10.55 [a], 10.66 [e])	10.55 (10.55 [a], 10.66 [e])	10.55 (10.55 [a], 10.66 [e])	0.122 (0.123 [b], 0.087 [a])	0.41 (0.42 [a])

[a] Cal. data from Min et al. [18]. [b] Exp. Lattice parameters from [8]. [c] Exp. Lattice parameters from Ref [20]. [d] Exp. Lattice parameters from Ref [21]. [e] Exp. Lattice parameters from Ref [22].

The influence of applied pressure on the crystal structure of Cr_7C_3, Cr_3C_2 and $Cr_{23}C_6$ phases, the variation in the lattice parameters ratio (a/a_0, b/b_0, c/c_0) and unit cell volume rate (V/V_0) with respect to pressure are plotted in Figure 2a–d, where a_0, b_0, c_0 and V_0 are the zero-pressure equilibrium lattice parameters and volume.

It can be clearly observed that the ratio of V/V_0 decreased along with increased pressure, which indicates that the crystal structure of each binary carbide undergoes a certain compression. Besides, authors compared the compressibility of W, Al, Si pure elements, which are always used as a matrix for chromium carbide composite. It can be seen that W metal displays closer compressibility trends with three binary carbides, while aluminum and silicon are much softer. At 10 GPa, the volume of Cr_7C_3, Cr_3C_2 and $Cr_{23}C_6$ was reduced by 3.05%, 2.89% and 3.12%, respectively, implying that Cr_3C_2 has optimal structural stability under applied pressure. The declining trend of a/a_0 is obvious in the case of Cr_3C_2, which can be attributed to the longer Cr-C bond length along a-axis and the weaker bond strength. Similarly, the c/c_0 of Cr_7C_3 shows a similar trend.

The chemical bonding properties of binary chromium carbides under hydrostatic pressure are also discussed in Figure 2e–g. The chemical bonds, which are easy to change with pressure, are situated on the higher part of the graphs, showing a stronger dependence on pressure. The same type of bond V in Cr_7C_3 and bond IV in Cr_3C_2 are stiff and exhibit

the smallest compressibility among all chemical bonds. Several different bond lengths are observed in binary chromium carbides and overall the variation trend remained. It can also be found that the bonds aligned along the (001) plane exhibit higher compressibility than other chemical bonds.

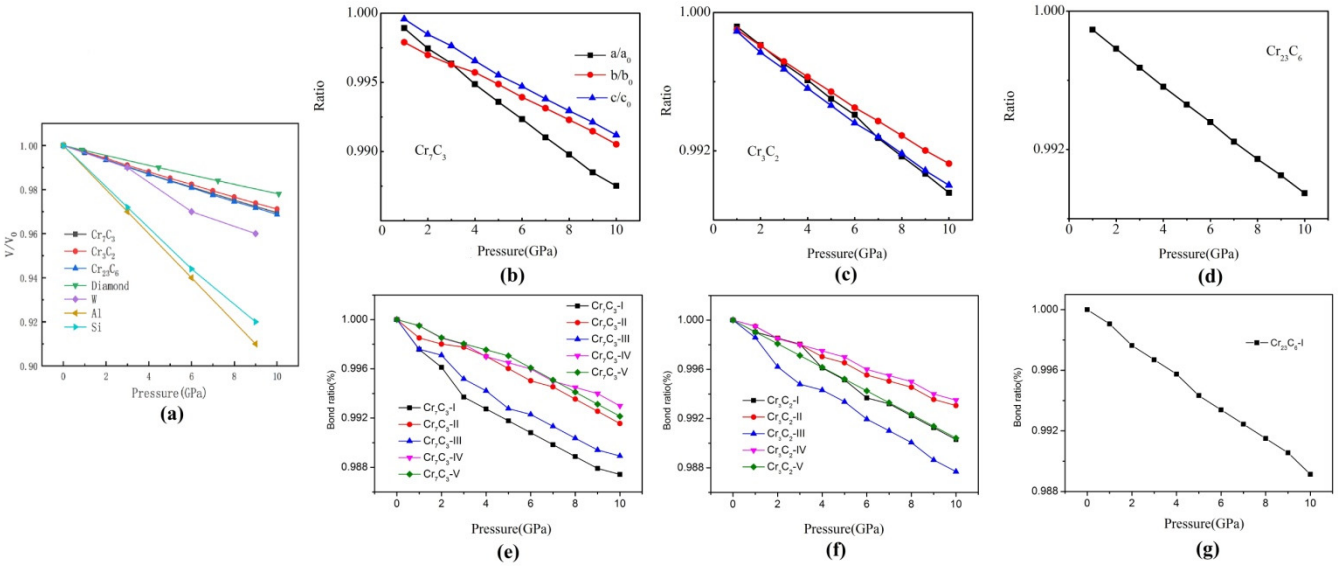

Figure 2. The chemical bonding properties of binary chromium carbides under hydrostatic pressure: (**a**) the unit cell volume rate (V/V_0), (**b**) lattice parameters ratio (a/a_0, b/b_0, c/c_0) of Cr_7C_3, (**c**) lattice parameters ratio (a/a_0, b/b_0, c/c_0) of Cr_3C_2, (**d**) lattice parameters ratio (a/a_0, b/b_0, c/c_0) of $Cr_{23}C_6$, (**e**) the chemical bonding properties of Cr_7C_3 under hydrostatic pressure, (**f**) the chemical bonding properties of Cr_3C_2 under hydrostatic pressure, (**g**) the chemical bonding properties of $Cr_{23}C_7$ under hydrostatic pressure [23].

3.2. Formation Enthalpy

The formation enthalpy (ΔH) of binary chromium carbides has been calculated to evaluate the structural stability. The formation enthalpy is defined as the change in energy to form 1 M of any substance and a lower formation enthalpy indicates better forming ability. The formation enthalpy of a single cell is given below:

$$\triangle H = \frac{E_{total}(\mathrm{Cr}_x\mathrm{C}_y) - xE_{bulk} - yE_{bulk}(\mathrm{C})}{x+y} \quad (1)$$

In Equation (1), E_{total} ($\mathrm{Cr}_x\mathrm{C}_y$) represents the total cell energy; E_{bulk}(Cr) and E_{bulk}(C) refer to the chemical potential of Cr, C atoms in the bulk state; x and y correspond to the number of Cr, C atoms in each cell, respectively. Generally, the value of $\Delta H < 0$ implies that binary chromium carbides are structural stable. It can be seen from Table 1 that the formation enthalpy of Cr_7C_3, Cr_3C_2 and $Cr_{23}C_6$ is -0.157, -0.183 and -0.122 eV·atom^{-1} without pressure, respectively. Therefore, the binary chromium carbides are structurally stable with a stability sequence of Cr_3C_2 > Cr_7C_3 > $Cr_{23}C_6$.

To investigate the structural stability of binary chromium carbides under pressure, the formation enthalpy of binary chromium carbides under elevated pressure ranging from 0 to 10 GPa is calculated and plotted in Figure 3. It can be seen that the formation enthalpy increased along with pressure, suggesting a lower structural stability in the binary phases. Furthermore, the initial growth (from 1 to 4 GPa) is more obvious than the latter (from 5 to 10 GPa), and the formation enthalpy of Cr_3C_2 kept on increasing, whereas the ΔH values for Cr_7C_3 and $Cr_{23}C_6$ remained at the pressure of 5–10 GPa.

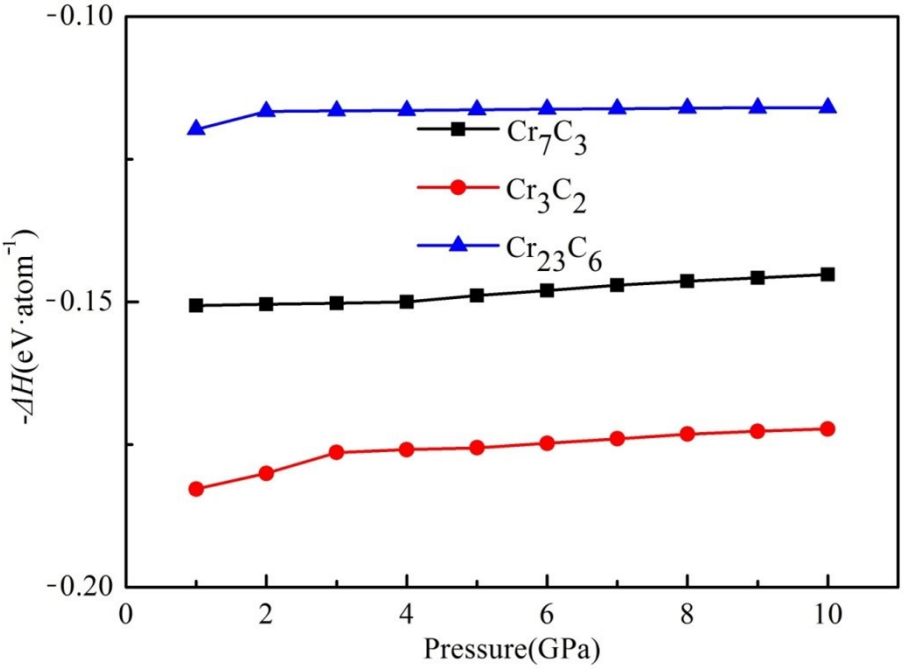

Figure 3. The formation enthalpy of binary chromium carbides under elevated pressure.

Although the formation enthalpies of three compounds experienced a certain reduction, the negative values below 10 GPa indicate the structural stability of the three compounds. Moreover, Cr_3C_2 has exhibited the highest structural stability with a formation enthalpy of -0.172 eV·atom $^{-1}$ at 10 GPa.

3.3. Electronic Structures

The values of total density of states of binary chromium carbides at Fermi level N (D_f), without any applied pressure, are shown in Table 1. The D_f values of 0.42, 0.36 and 0.41 state/(eV·atom) are observed for Cr_7C_3, Cr_3C_2 and $Cr_{23}C_6$, respectively. Moreover, the positive values of D_f indicates the metallic character of these compounds. Among them, the lower D_f value of Cr_3C_2 confirms that it has the weakest metallic behavior and highest structural stability, which is consistent with our formation enthalpy data.

To further understand the basic features of the chemical bonding and phase stability, the total and partial density of states (DOS) of binary chromium carbides were calculated and shown in Figure 4. The main bonding peaks of binary chromium carbides, between -75 and -70 eV, are dominated by the valence electron number of the Cr (3*s*) orbit, while the main bonding peaks between -45 and -40 eV originated from the valence electron number of the Cr (3*p*) orbit. In addition, both of them have exhibited a strong local behavior. Meanwhile, the low energy region of three compounds between -14 and -10 eV is determined by the valence electron number of the C (2*s*) orbit, while among the high energy region, from -7 to -3 eV, this is contributed by Cr (3*d*) and C (2*p*) orbits, indicating that the covalent hybridization between the Cr and C atoms exits in these compounds. Moreover, the Cr (3*d*) predominates near the Fermi level stems because of its metallic characteristics.

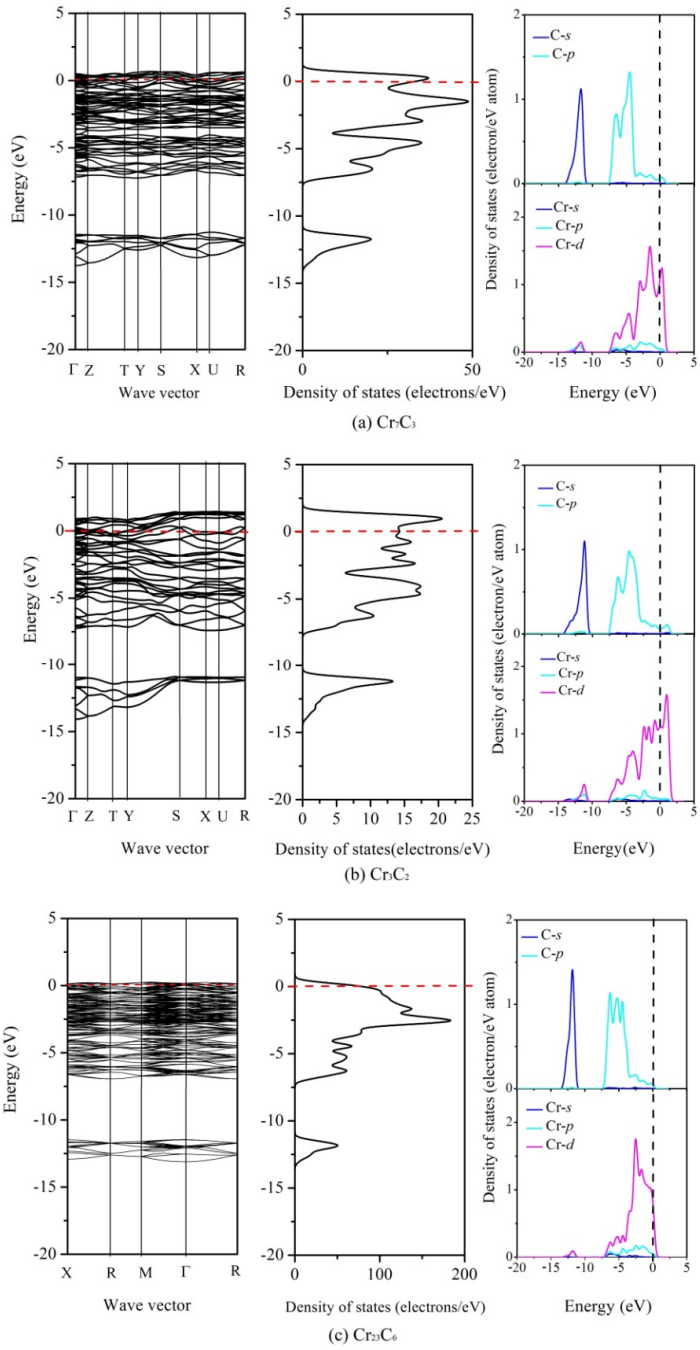

Figure 4. The total and partial density of states (DOS) of binary chromium carbides without applied pressure.

Figure 5 presents that the calculated value of the total DOS at Fermi level N (D_f) decreases under pressure, which suggests that the metallic nature of Cr_7C_3, Cr_3C_2 and $Cr_{23}C_6$ reduced due to applied pressure. This probably attributes to the bond length of atoms, which becomes shorter under high pressure, and alters the interaction potentials. In addition, a pseudo-gap exists around the Fermi level and becomes wider under applied pressure. In general, the wider pseudo-gap represents a stronger covalent bond, which is in good agreement with our calculations.

Furthermore, the partial DOS under pressure (0, 5 and 10 GPa) is calculated and shown in Figure 6. It can be seen the partial DOS, especially for the Cr atom, decreased along with increasing pressure, which can be attributed to the reduced distance between atoms, wider pseudo-gaps, and higher bond strength of Cr-C.

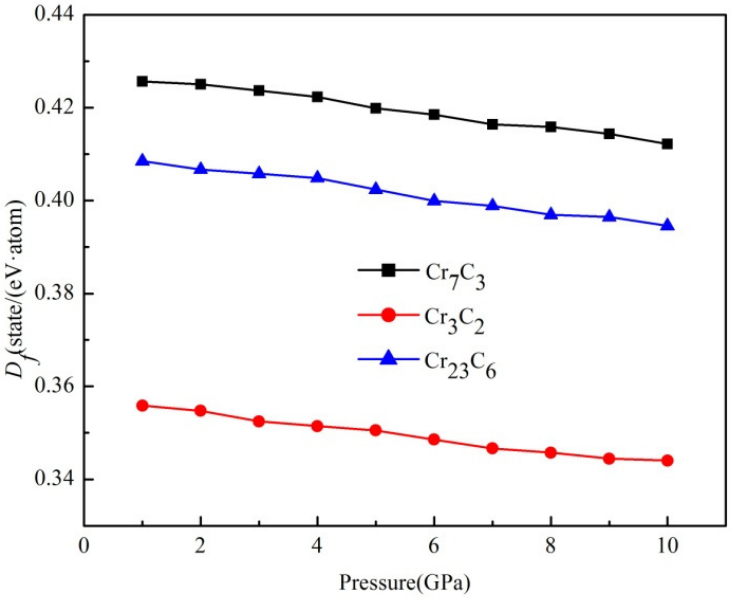

Figure 5. The value of the total DOS at Fermi level N (D_f) decreases under pressure.

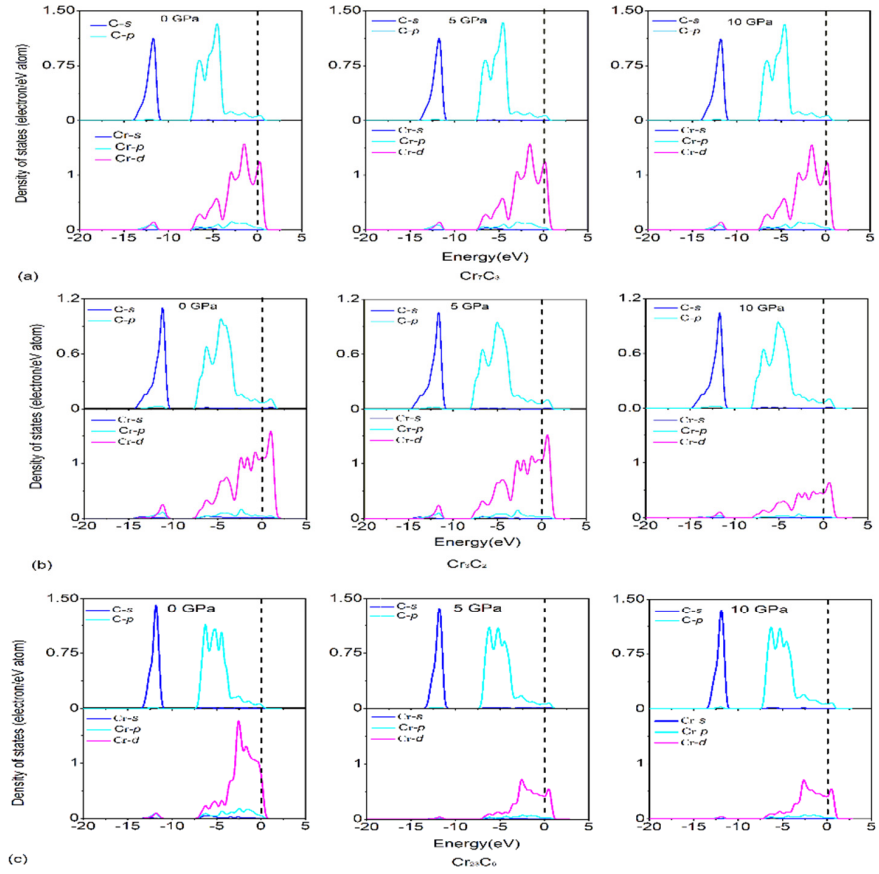

Figure 6. The partial DOS of (**a**) Cr_7C_3, (**b**) Cr_3C_2 and (**c**) $Cr_{23}C_6$ under pressure (0, 5 and 10 GPa).

In order to visually demonstrate the covalent and ionic bonding characteristics, the charge density difference was measured and results are shown in Figure 7. The contour lines are plotted from -1 to 1 e/Å^3. It can be clearly observed that the bonding type between C and Cr is covalent, the bonding between adjacent Cr atoms is metallic, whereas the bonding around C atoms is ionic. Based on the above results, it can also be seen that binary chromium carbides have strong structural stability.

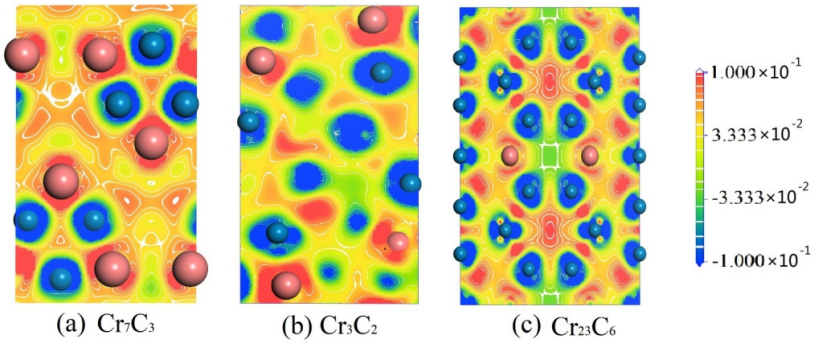

Figure 7. The charge density difference of three binary chromium carbides.

Figure 8 shows the charge density difference of Cr_7C_3, Cr_3C_2 and $Cr_{23}C_6$ under different applied pressures (0, 5 and 10 GPa). It can be seen that the blue region surrounding Cr atoms decreased along with increasing pressure, which indicates that the energy difference between Cr and C atom shows a certain decrease. Moreover, it implies that the covalent bond becomes stronger due to the orbital hybridization. The color contrast of Cr_3C_2 clearly demonstrates that the covalent bond of Cr_3C_2 is the strongest among the chromium carbides.

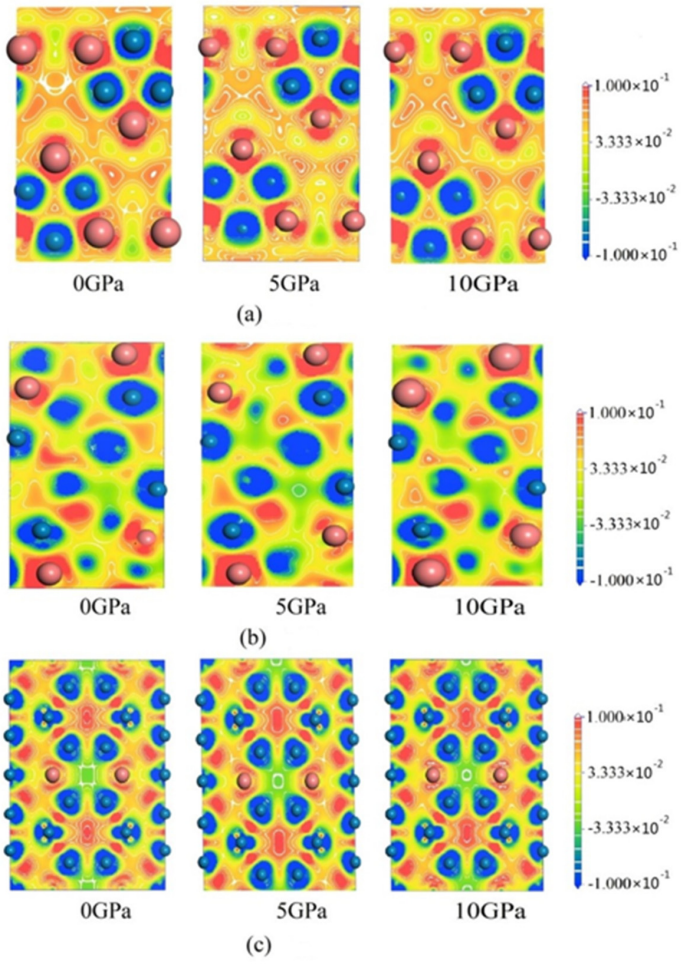

Figure 8. The charge density difference of (**a**) Cr_7C_3, (**b**) Cr_3C_2 and (**c**) $Cr_{23}C_6$ under different applied pressures.

3.4. Mechanical Characterizations

The mechanical properties of binary chromium carbides, such as elastic modulus and hardness are of critical importance in the wear resistance of surface coating materials. Moreover, most of the elastic properties remain almost in direct correlation with the elastic constants. In this work, the elastic constants of binary chromium carbides are calculated by the stress-strain approach and results are presented in Table 2. The mechanical stability criteria are expressed below [24–30]:

For orthorhombic system (Cr_7C_3, Cr_3C_2)

$$C_{11} + C_{12} + C_{33} + 2C_{12} + 2C_{13} + 2C_{23} > 0,$$

$$C_{11} + C_{22} > 2C_{12}, C_{22} + C_{33} > 2C_{23},$$

$$C_{11} + C_{33} > 2C_{13}, C_{ii} > 0 \text{ (I = 1-6)}$$

For cubic system ($Cr_{23}C_6$):

$$C_{11} > 0, C_{44} > 0, C_{11} - C_{12} > 0, C_{11} + 2C_{12} > 0.$$

Table 2 confirms that chromium carbides have a mechanically stable structure because all binary Cr-C systems satisfy the stability criteria. Moreover, the results are consistent with other theoretical results. The mechanical properties, such as bulk modulus (B), shear modulus(G) and Young's modulus (E), are obtained by using Voigt-Reuss-Hill (VRH) approximation, which considers the average of the bounds and provides the best estimation for mechanical properties of polycrystalline materials from known elastic constants of a single crystal [24]:

$$B_{VRH} = \frac{1}{2}(B_V + B_R) \quad (2)$$

$$G_{VRH} = \frac{1}{2}(G_V + G_R) \quad (3)$$

$$E = \frac{9B_{VRH}G_{VRH}}{(3B_{VRH} + G_{VRH})} \quad (4)$$

$$v = \frac{(3B_{VRH} - 2G_{VRH})}{2(3B_{VRH} + G_{VRH})} \quad (5)$$

where B_V, B_R and B_{VRH} represent the bulk modulus calculated by Voigt, Reuss and Voigt-Reuss-Hill approximation, respectively. Similarly, G_v, G_R and G_{VRH} correspond to the shear modulus calculated from Voigt, Reuss and Voigt-Reuss-Hill approximation, respectively. E refers to the Young's modulus and ν represents the Poisson's ratio. The values of B, G, E and ν for Cr_7C_3, Cr_3C_2 and $Cr_{23}C_6$ at zero pressure are presented in Table 2, and are in good agreement with other theoretical results. B represents the resistance to fracture and Cr_7C_3, Cr_3C_2 and $Cr_{23}C_6$ resulted in B values of 314.7, 341.7 and 296.1 GPa, respectively. G represents the resistance to plastic deformation and Cr_3C_2 exhibited the maximum value of G. Furthermore, the B/G ratio is generally used to assess the ductile or brittle nature of materials. If B/G value is less than 1.75, the materials exhibit brittle behavior; whereas for $B/G > 1.75$, the material demonstrate ductile nature. E refers to the resistance to compression or tensile resistance, and Cr_7C_3, Cr_3C_2 and $Cr_{23}C_6$ have delivered E values of 353.4, 423.7 and 377.9 GPa, respectively. It is worth noting that these E values are higher than $3Al_2O_3$-SiO_2 (145 GPa) [34,35], ZrO_2(160–241 GPa) [35], $MgAl_2O_4$(240 GPa) [35], Si_3N_4 (220–320 GPa) [36], and AlN(310–350 GPa) [36], and lower than TiC(379 GPa) [36], WC(400–650 GPa) [36], WC-Co(400–530 GPa) [36], diamond(1000 GPa) [36–38]. In brief, the Cr_3C_2 compound has demonstrated the highest values of B, G and E, which indicate that Cr_3C_2 has the greatest resistance to deformation.

Table 2. Calculated values of the independent elastic constants (C_{ij}), C_{11}/C_{33}, C_{12}/C_{13}, C_{44}/C_{66}, bulk module (*B*, GPa), shear module (*G*, GPa), Young module (*E*, GPa), and Poisson's ratio (*v*) at zero pressure.

Phase	C_{11}/GPa	C_{12}/GPa	C_{13}/GPa	C_{22}/GPa	C_{23}/GPa	C_{33}/GPa	C_{44}/GPa	C_{55}/GPa	C_{66}/GPa
Cr_7C_3	459.9 (410.1, [c] 409) [a]	262.7 (252, [a] 241.1) [c]	251.0 (227, [a] 203.7) [c]	512.6 (441, [c] 376) [a]	280.2 (333, [a] 257.3) [c]	525.1 (459.5, [c] 409) [a]	186.2 (168, [c] 145) [a]	142.9 (124.3, [c] 123) [a]	114.2 (108.3, [c] 82) [a]
Cr_3C_2	463.0 (484, [a] 447.1) [c]	212.5 (229, [a] 217.5) [c]	228.2 (243.3, [c] 243) [a]	543.6 (554, [a] 545.3) [c]	227.5 (244, [a] 217.9) [c]	495.3 (491, [a] 471.2) [c]	235.8 (237.7, [c] 230) [a]	116.1 (116.6, [c] 111) [a]	240.0 (241.3, [c] 235) [a]
$Cr_{23}C_6$	486.3 (487, [f] 481, [a] 473.8) [c]	201.0 (209, [a] 200, [f] 186.6) [c]					149.6 (149, [f] 146.7, [c] 138) [a]		
Phase	C_{11}/C_{33}	C_{12}/C_{13}	C_{44}/C_{66}	B/GPa	G/GPa	*B*/*G*	*E*/GPa	*v*	
Cr_7C_3	0.88	1.05	1.63	341.7 (312, [a] 311.7, [e] 309, [b] 300.6) [c]	133.1 (143.9, [d] 118.0, [c] 82) [a]	2.57 (2.55) [a]	353.4 (374, [e] 371, [b] 313.0, [c] 226) [a]	0.33 (0.38, [a] 0.33) [c]	
Cr_3C_2	0.94	0.93	0.98	314.7 (329, [a] 312.9) [c]	166.1 (162.1, [c] 162) [a]	1.89 (1.93) [a]	423.7 (416, [a] 414.7) [c]	0.28 (0.29, [a] 0.28) [c]	
$Cr_{23}C_6$	1.00	1.00	1.00	296.1 (300, [a] 282.3) [c]	146.8 (145.4, [c] 137) [a]	2.02 (1.94) [a]	377.9 (372.3, [c] 357) [a]	0.29 (0.30, [a] 0.28) [c]	

[a] Exp. data from H. Kleykamp [8]. [b] Cal. data from Music et al. [7]. [c] Cal. data from Min et al. [18]. [d] Cal. data from Price et al. [31]. [e] Cal. data from Xiao et al. [32]. [f] Exp. data from Henriksson et al. [33].

In addition, the values of B, G and E of Cr_7C_3, Cr_3C_2 and $Cr_{23}C_6$ under applied pressure are also calculated and presented in Figure 9. The calculated moduli have shown a certain similarity and a direct relationship with increase with pressure. In terms of B, the initial rate of growth, from 0 to 4 GPa, is less steep than the latter part, from 5 to 10 GPa. Moreover, the resistance to pressure becomes higher along with the elevated pressure. Furthermore, the values of G are lower than those of B from 0 to 10 GPa, which implies that the shear modulus limits the structural stability. In case of Young's modulus, the growth rate for Cr_3C_2 was steeper than for Cr_7C_3 and $Cr_{23}C_6$, which can be attributed to the larger volumetric variations of Cr_3C_2 under applied pressure (Figure 2).

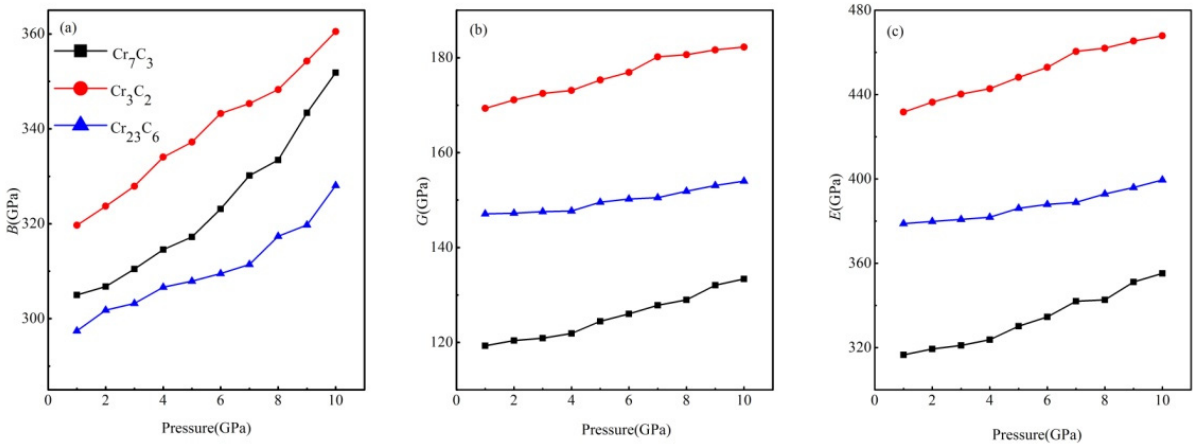

Figure 9. The values of (**a**) B, (**b**) G and (**c**) E of Cr_7C_3, Cr_3C_2 and $Cr_{23}C_6$ under applied pressure.

Meanwhile, hardness is an important index to assess wear resistance of ceramic materials. The hardness of a ceramic material has a certain relationship with its composition and microstructure. According to Gao's theory [27], the theoretical hardness can be calculated by using the given empirical formulae:

$$H = [\prod^{u} (H_v^u)^{n^u}]^{1/\sum n^u} \tag{6}$$

$$H_v^u(GPa) = 740 P^u (v_b^u)^{-(5/3)} \tag{7}$$

$$v_b^u = \frac{(d^u)^3}{\sum_v \left[(d^v)^3 N_b^v\right]} = \frac{(d^u)^3}{\sum_v \left[(d^v)^3 \frac{N^v}{\Omega}\right]} = \frac{(d^u)^3 \Omega}{\sum_v \left[(d^v)^3 N^v\right]} \tag{8}$$

where H refers to the theoretical hardness of compound, H_v^u represents the hardness of u type bond, d^u corresponds to the bond length, H_v^u refers to the v type bond density per cubic angstroms; N^v represents the total number of v type bonds in the cell, and P^u and Ω correspond to the overlap population of u type bond and cell volume, respectively.

The overlap population of each atom is shown in Table 3. The difference of atomic position in three binary Cr-C systems resulted in few gaps in the gains and losses of Cr and C atoms. Total refers to the total electron number after the gains and losses; ***Charge*** refers to the gains and losses in electron number, where negative value indicates the electron gains and vice versa, and summation of both values provides the original electron number, such as 4.53 + (−0.53) = 4. It is well-known that the bigger overlap population of electron clouds implies the better capacity of a covalent bond, which confirms that Cr_3C_2 has the strongest covalent bond.

Table 3. Atomic orbit population of Cr_7C_3, Cr_3C_2 and $Cr_{23}C_6$ at zero pressure.

Phase	*Species*	*s*	*p*	*d*	*Total*	*Charge*(*e*)
Cr_7C_3	C	1.38	3.16		4.53	−0.53
	C	1.38	3.17		4.55	−0.55
	Cr	2.08	6.66	5.01	13.74	0.26
	Cr	2.09	6.69	5.00	13.78	0.22
	Cr	2.07	6.76	5.00	13.82	0.18
Cr_3C_2	C	1.40	3.09		4.49	−0.49
	C	1.40	3.11		4.51	−0.51
	Cr	2.13	6.61	4.96	13.70	0.30
	Cr	2.14	6.54	4.99	13.67	0.33
	Cr	2.15	6.50	4.98	13.63	0.37
$Cr_{23}C_6$	C	1.38	3.21	5.00	13.90	−0.59
	Cr	2.17	6.73	5.00	13.86	0.10
	Cr	2.10	6.76			0.14

The calculated hardness of each Cr-C bond and binary chromium carbide, without external pressure, is shown in Table 4. The theoretical hardness of Cr_7C_3, Cr_3C_2 and $Cr_{23}C_6$ was found to be 13.5, 18.2 and 10.1 GPa, respectively. The difference in hardness stems from the difference in Cr-C bond strength and bond density. In spite of the lower bond density, the Cr_3C_2 compound has exhibited the highest hardness value and maximum Cr-C bond strength. The calculated results are in good agreement with the experimental studies [15]. However, the hardness values are lower than the values calculated by Min Ting et al. [18], where the semi-empirical formula of Šimůnek has been used to the calculate the hardness values [25]. This might have happened due to the computational difference in cell volume and Cr-C bond strength. However, it is worth emphasizing that our samples have shown a similar sequence for three compounds: Cr_3C_2 > Cr_7C_3 > $Cr_{23}C_6$. This implies that our results are acceptable based on a different calculation method.

Table 4. The volume of unit cell (Ω, Å^3) the v type bond density per Å^3(N_b^v), the hardness of u type bond (H_v^u, GPa) and theoretical hardness (H, GPa) of Cr_7C_3, Cr_3C_2 and $Cr_{23}C_6$ at zero pressure.

Phase	**Bond**	**Ω(Å^3)**	N_b^v	H_v^u/GPa	H_{Gao}/GPa
Cr_7C_3	C-Cr	364.74	0.192	17.27	13.5
	C-Cr			17.19	(18.3 [a])
	C-Cr			15.55	
	C-Cr			14.81	
	C-Cr			14.50	
Cr_3C_2	C-Cr	175.47	0.160	13.67	18.2
	C-Cr			29.03	
	C-Cr			27.25	(20.9 [a])
	C-Cr			22.35	
	C-Cr			19.81	
	C-Cr			8.46	
	C-Cr			8.17	
$Cr_{23}C_6$	C-Cr	1178.28	0.163	11.24	10.1
	C-Cr			9.07	(13.2 [a])

[a] Cal. data from Min et al. [18].

Moreover, most of the carbide ceramics exhibit high hardness values, such as FeC (8.4 GPa) [10], TaN (11.0 GPa) [10] and NbN (13.3 GPa) [10], Mo_2C (15.5 GPa) [10], TaC (16.7 GPa) [10] and NbC (19.6 GPa) [10], CrB_2 (20.5 GPa [10], 23.0 GPa) [10] and VC (27.2 GPa) [10], α-B_4C_3 (60 GPa) [13] and c-B_4C_3 (65 GPa) [13]. One should note that the hardness values, achieved for binary chromium carbides, are reasonably high and located in the middle of this spectrum.

Furthermore, the materials should deliver high hardness under high-pressure environments. Hence, the hardness values under applied pressure are calculated, and the

H/H_0 ratio is used to characterize the change in hardness, where H_0 refers to the hardness without external pressure. Figure 10 presents the relationship between H/H_0 and applied pressure. It can be clearly observed that hardness values linearly increased with applied pressure, which can be attributed to the increase in bond density and shortened bond length. Moreover, the variation in H/H_0 of Cr_3C_2 is more obvious than the Cr_7C_3 and $Cr_{23}C_6$, which shows that the influence of Cr-C bond strength and the density of Cr_3C_2 play a remarkable role. Cr_3C_2 has exhibited the highest strength under applied pressure. These calculations provide the theoretical basis for the development and utilization of chromium carbides, particularly Cr_3C_2, for a wide range of applications.

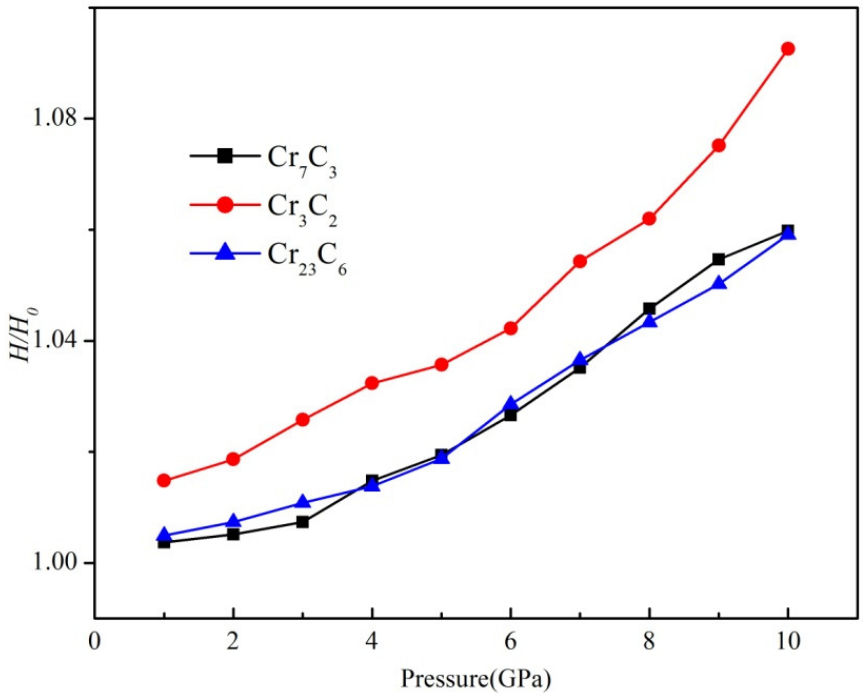

Figure 10. The relationship between H/H_0 and applied pressure.

Hardness anisotropy also provides guidelines to fabricate the hardest cutting tools. Generally, machine components are desirable with cutting angle accuracy and specific shape. The hardest facets are designed to interface and orient with the machine component, which substantially enhances the service life of cutting tools. According to the Li' theory, anisotropic hardness can be computed from the given equations [37–39]:

$$Hani = \left[\prod_{i=1}^{j} H_i^{ni}\right]^{1/\sum_{i=1}^{j} ni} \quad (9)$$

$$Hi = a\delta_{t(i)}^{b}\rho_i^{c} \quad (10)$$

$$\rho_i = n_i / V_i \quad (11)$$

$$V_i = n_i d_i^3 \;\; V / \sum_{k=1}^{j} n_k d_k^3 \quad (12)$$

where i represents the ith department, n_i refers to the bond number, δt^{i} represents the total band strength, ρ_i corresponds to the bond density, V_i represents the volume, and d_i refers

to the bond length. The constants a, b, c take the value of 1.5, 1 and 0.5 for Vickers hardness, and 1.3, 1 and 0.5 for Knoop hardness. δ_t can be obtained from the given equation [39]:

$$\delta_t = \frac{\delta_s \delta_b}{\delta_s \sin^2 \varphi + \delta_b \cos^2 \varphi} \tag{13}$$

where φ refers to the angle between a specific bond and designated crystallographic direction or crystallographic plan, and the average values of $\sin\varphi$ and $\cos\varphi$ are $\pi 4$ and $1/2$, respectively. δ_s and δ_b correspond to the stretching strength and bending strength, respectively, and can be obtained from the given relationships [39]:

$$\delta_s = 26.9 \frac{\chi_A \chi_B}{d^{0.5}} \tag{14}$$

$$\delta_b = 33.5 \frac{\chi_A \chi_B}{d^2} e^{-9.7 fw} \tag{15}$$

where z represents the charge transfer number between bonded atoms A and B. The calculated anisotropic hardness values of binary chromium carbides are presented in Table 5. Overall, Cr_7C_3 exhibited the highest hardness due to shorter bond length and maximum bond density. For Cr7C3, the hardness in [110] direction is higher than other directions. Moreover, the hardness in [100] direction is higher than [010] and [001] directions, which are perpendicular to the a-axis. This phenomenon can be attributed to the bond angle. For example, the shortest bond of Cr7C3 is the Cr-C bond, which has a bond length of 1.974 Å. The Cr-C bond makes an angle of 23.391°, 69.479° and 87.38° with [100], [010] and [001] directions, respectively. It is worth noting that the smaller angle results in stronger δt which consequently results in higher hardness. Moreover, the hardness along [110] and [111] directions are similar to the average hardness, which is probably due to higher Cr-C covalent bonds in these directions as compared to the {110} family. In addition, the maximum covalent bonds are located in (110) plane. For Cr3C2, the hardness values along the given directions are consistent with the average hardness, which indicates that Cr-C bonds are homogeneously distributed. Hence, owing to excellent structural stability and mechanical performance, Cr3C2 has potential to be used in a wide range of applications, such as cutting tools and wear-resistant coatings. For Cr23C6, hardness remarkably dispersed along given directions, and the hardness value along [001] matches the overall hardness, though the average calculated hardness is higher than the previously published reports [12–15,40–45].These data are the first to provide prediction of hardness anisotropy for binary chromium carbides.

Table 5. The calculated anisotropic hardness of binary chromium carbides.

Phase	Chemical Bond	H_{vani}/GPa					f_w	H_v/ GPa
		[100]	[010]	[001]	[110]	[111]		
Cr_7C_3	Cr-C	24.93	24.16	21.05	**26.53**	25.79	0.019	26.17
Cr_3C_2	Cr-C	22.78	21.47	21.57	22.23	**24.16**	0.019	23.30
$Cr_{23}C_6$	Cr-C	16.42	15.18	**21.91**	17.86	21.15	0.041	19.09

χ_A and χ_B represent the electronegativity of atoms of A and B, respectively, and f_w refers to the strength weakening factor, which can be expressed as:

$$f_w = \frac{|\chi_A - \chi_B|}{z^2(\chi_A - \chi_B)} \tag{16}$$

To investigate the variation in anisotropic hardness with respect to applied pressure, the hardness values were calculated in a different direction, under the pressure of 1–10 GPa, and results are presented in Figure 11. Overall, the hardness values have shown a direct relationship with applied pressure. For Cr7C3, the increase in hardness value along [001] is

most significant, whereas the minimum hardness value was observed along [001] direction at 0 GPa. This can be attributed to a relatively higher initial bond length, which becomes noticeably shorter with the reduction in crystal trend. Moreover, the hardness value along [010] direction in Cr3C2 and Cr23C6 has shown a similar condition. However, some differences have also been observed among three compounds. For instance, the rate of hardness increases along [110] was higher and steeper than the rate along [010] and [001] directions for Cr7C3, in the pressure range of 1–3 GPa. However, it becomes normal in the pressure range of 3–10 GPa, which is mainly due to the bond length along the [110] direction. The higher rate results in reduced amplitude of the inherent short bond, smaller than those bonds. For Cr_3C_2 and $Cr_{23}C_6$, the ratio curves exhibited a constant trend. In summary, the hardness of Cr_3C_2 has a relatively balanced increase compared to Cr_7C_3 and hardness value of Cr_3C_2 are higher than for $Cr_{23}C_6$, which confirms the desirable mechanical properties of Cr_3C_2.

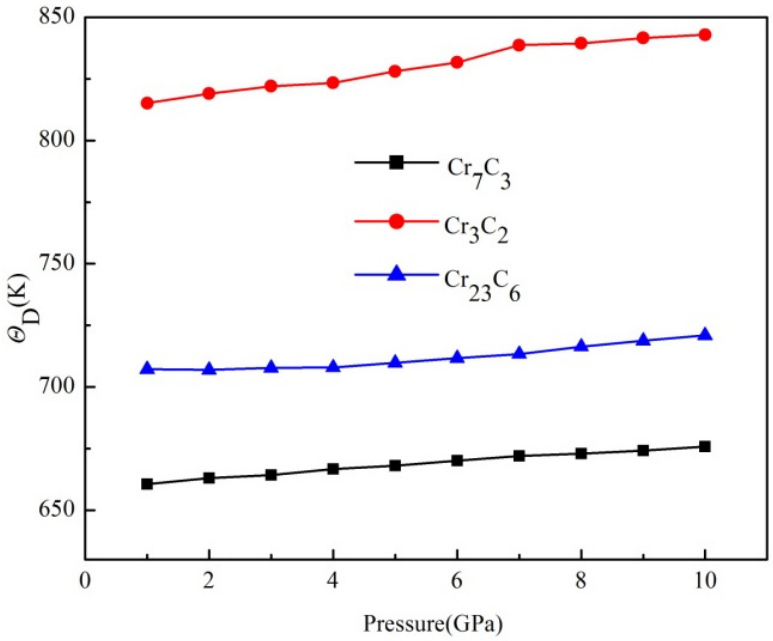

Figure 11. The variation in anisotropic hardness with respect to applied pressure.

3.5. Thermodynamic Stability

Debye temperature (Θ_D) is the critical temperature applied in the energy equalization theorem. According to the Debye Law of solid physics, the specific heat tends to become 0 at extremely low temperatures and energy equalization is achieved if $T > \Theta_D$ [17]. To analyze the thermodynamic stability of binary chromium carbides, the Debye temperatures (Θ_D) are calculated in this section. The Debye temperature has a certain correlation with many physical properties, such as melting point, elastic modulus and specific heat. Generally, the average sound velocity (v_m) is used to calculate the Debye temperature, according to the given equation [46–49]:

$$\Theta_D = \frac{h}{k_B}\left[\frac{3n}{4\pi}\left(\frac{\rho N_A}{M}\right)\right]^{\frac{1}{3}} v_m \tag{17}$$

where h refers to the Planck's constant; k_B represents the Boltzmann constant; N_A corresponds to the Avogadro constant; n refers to the total number of atoms per formula; ρ represents the density; and M is the relative molecular mass per compound. v_m can be calculated from the following expression:

$$v_m = \left[\frac{1}{3}\left(\frac{2}{v_s^3} + \frac{1}{v_1^3}\right)\right]^{-\frac{1}{3}} \tag{18}$$

where v_1 and v_s represent the longitudinal and transverse sound velocities, respectively, which are calculated from the Navier's formulas [50]:

$$v_1 = \sqrt{(B + \frac{4}{3}G)\frac{1}{\rho}},\ v_s = \sqrt{G/\rho} \tag{19}$$

The calculated results of Θ_D, v_1. and v_s are listed in Table 6. The Θ_D is used to characterize the strength of covalent bonds in solids. It can be observed that the higher Θ_D of 850 K was achieved for Cr_3C_2, which confirms the presence of strong covalent bonds in Cr_3C_2. This observation is consistent with our mechanical characterization data, where Cr_3C_2 has shown higher mechanical properties as compared to Cr_7C_3 and $Cr_{23}C_6$. In addition, the higher Debye temperature implies that thermal stability of Cr_3C_2 is higher than the other two compounds.

Table 6. Theoretically calculated thermal properties of chromium carbides, including $v_1(\mathrm{m{\cdot}s^{-1}})$, $v_s(\mathrm{m{\cdot}s^{-1}})$, $v_m(\mathrm{m{\cdot}s^{-1}})$ and Θ_D(K) at zero pressure.

Phase	v_1/m·s^{-1}	v_s/m·s^{-1}	v_m/m·s^{-1}	Θ_D/K
Cr_7C_3	10,894.29(8051.65 [a])	5516.13(4087.19 [a])	6183.41(4580.90 [a])	731(785 [a], 646 [b])
Cr_3C_2	11,447.63(8812.80 [a])	6371.63(4878.25 [a])	7095.38(5343.72 [a])	850(785 [a], 785 [b])
$Cr_{23}C_6$	10,692.17(8152.31 [a])	5841.449(4504.88 [a])	6514.34(5019.43 [a])	744(691 [a], 671 [b])

[a] Cal. data from Min et al. [18]. [b] Cal. data from Jang C et al. [9].

To study the influence of applied pressure on the thermodynamic stability of the binary chromium carbides, Θ_D of binary chromium carbides, under external pressure, is calculated and presented in Figure 12. It can be found Θ_D gradually increased along with increasing pressure, which implies the higher thermodynamic stability of Cr_7C_3, Cr_3C_2 and $Cr_{23}C_6$. The Θ_D curves have shown a constant trend and the growth curve of Cr_3C_2 was relatively definite, which suggests that the thermodynamic stability of Cr_3C_2 is better than other two compounds. This result provides an insight into the highest bulk modulus of Cr_3C_2, which is correlated with the resistance to volumetric deformations. In brief, the Cr_3C_2 has exhibited the best mechanical and thermodynamic properties among the three binary Cr-C systems.

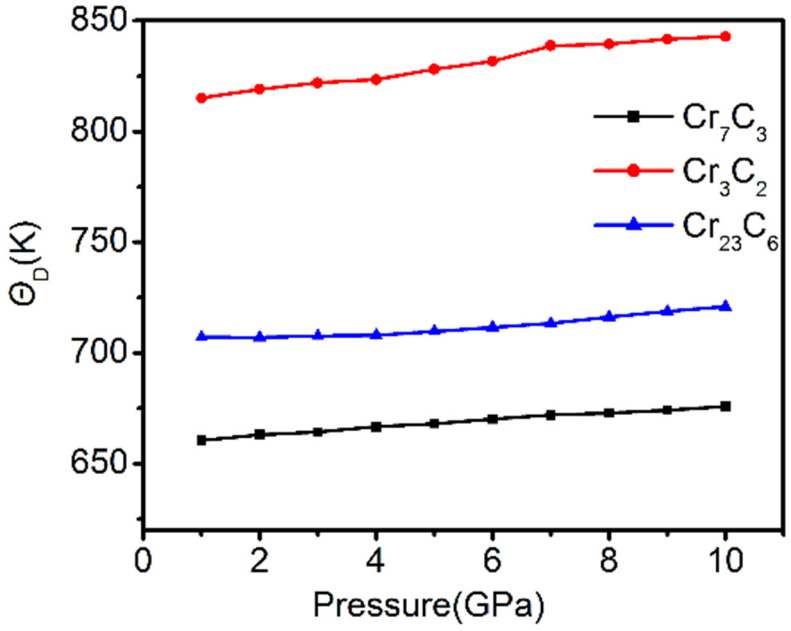

Figure 12. Θ_D of binary chromium carbides under external pressure.

4. Conclusions

Herein, we have carried out an ab initio study of binary chromium carbides, under applied pressure, by using first-principles based on density functional theory and evaluated the crystal structure, electronic structure, mechanical performance and thermal properties. We have found that the V/V_0 ratio decreased along with increasing pressure, and the axial position, with longer bond length, is easier to compress. In terms of formation enthalpy, Cr_7C_3, Cr_3C_2 and $Cr_{23}C_6$ are structurally stable under applied pressure ranging from 0 to 10 GPa, and Cr_3C_2 has exhibited the best structural stability (minimal formation enthalpy). The electronic structure investigations revealed that the chemical bonds in Cr_7C_3, Cr_3C_2 and $Cr_{23}C_6$ are of a mixed type: stronger covalent bonds, ionic bonds and weaker metallic bonds. Moreover, the largest pseudo-gaps and higher bond strength were observed with increasing pressure. Cr_3C_2 has shown the strongest covalent bond. The values of moduli, B, G and E of Cr_7C_3, Cr_3C_2 and $Cr_{23}C_6$ under applied pressure increased, which imply that crystal structures are difficult to alter under elevated pressure. The hardness values of Cr_7C_3, Cr_3C_2 and $Cr_{23}C_6$ are 13.5, 19.2 and 10.1 GPa without any external pressure (0 GPa), and increased with increasing pressure. Similar to electronic and structural properties, the Cr_3C_2 has exhibited the best mechanical properties. Furthermore, we have studied the hardness anisotropy and concluded that the hardness values in [110], [111] and [001] are highest for Cr_7C_3, Cr_3C_2 and $Cr_{23}C_6$, respectively. In addition, the Cr-C bonds of Cr_3C_2 were homogenously distributed and hardness anisotropy was not obvious. The initial minimum hardness increased rapidly under the influence of external pressure, which is probably due to the contraction of Cr-C bonds around these directions. Finally, the Debye temperature (Θ_D) of Cr_7C_3, Cr_3C_2 and $Cr_{23}C_6$ are calculated and it has shown a direct relationship with pressure. These results confirm that binary compounds are thermodynamically stable.

Author Contributions: Conceptualization, L.S., L.Z.; methodology, X.J.; software, J.P.; formal analysis, W.Z.; investigation, H.D.; writing—original draft preparation, L.S.; writing—review and editing, L.X.; supervision, Y.L. All authors have read and agreed to the published version of the manuscript.

Funding: This work was supported by the Open Fund of State Key Laboratory for Mechanical Behavior of Materials (20192110 and 20202212), Natural Science Basic Research Plan in Shaanxi Province of China (2019JQ-821 and 2020JQ-777), the Open Fund of National Joint Engineering Research Center for Abrasion Control and Molding of Metal Materials (HKDNM201811 and HKDNM2019018), Scientific Research Program Funded by Shaanxi Provincial Education Department (20JK0837) and the Graduate Student Innovation and Practical Ability Training Program of Xi'an Shiyou University (YCS20212116).

Institutional Review Board Statement: Not applicable.

Informed Consent Statement: Not applicable.

Data Availability Statement: Not applicable.

Conflicts of Interest: The authors declare no conflict of interest.

References

1. Loubiére, S.; Laurent, C.; Bonino, J.P.; Rousset, A. Elaboration, microstructure and reactivity of Cr_3C_2 powders of different morphology. *Mater. Res. Bull.* **1995**, *30*, 1535–1546. [CrossRef]
2. Kok, Y.N.; Hovsepian, P.E. Resistance of nanoscale multilayer C/Cr coatings against environmental attack. *Surf. Coat. Technol.* **2006**, *201*, 3596–3605. [CrossRef]
3. Cheng, F.; Wang, Y.; Yang, T. Microstructure and wear properties of Fe-VC-Cr_7C_3 composite coating on surface of cast steel. *Mater. Charact.* **2008**, *59*, 488–492. [CrossRef]
4. Xie, J.; Chen, N.X.; Shen, J.; Teng, L.; Seetharaman, S. Atomistic study on the structure and thermodynamic properties of CrC, MnC, FeC. *Acta Mater.* **2005**, *53*, 2727–2732. [CrossRef]
5. Cintho, O.M.; Favilla, E.A.P.; Capocchi, J.D.T. Mechanical-thermal synthesis of chromium carbides. *J. Alloys Compd.* **2007**, *439*, 189–195. [CrossRef]

6. Sadangi, R.K.; McCandlish, L.E.; Kear, B.H.; Seegopaul, P. Synthesis and characterization of sub-micron vanadium and chromium carbide grain growth inhibitors. In Proceedings of the 1998 International Conference on Powder Metallurgy & Particulate Materials Sponsored by the Metal Powder Industries Federation and APMI International, Las Vegas, NV, USA, 31 May–4 June 1998.
7. Music, A.; Kreissig, U.; Mertens, R.; Schneider, J.M. Electronic structure and mechanical properties of Cr_7C_3. *Phys. Lett. A* **2004**, *326*, 473–476. [CrossRef]
8. Kleykamp, H. Thermodynamic studies on chromium carbides by the electromotive force (emf) method. *Alloys Compd.* **2001**, *321*, 138–145. [CrossRef]
9. Jiang, C. First-principles study of structural, elastic, and electronic properties of chromium carbides. *Appl. Phys. Lett.* **2008**, *92*, 041909. [CrossRef]
10. Čekada, M.; Panjan, P.; Maček, M.; ŠmíD, P. Comparison of structural and chemical properties of Cr-based hard coatings. *Surf. Coat. Technol.* **2002**, *152*, 31–35. [CrossRef]
11. Coltters, R.G.; Belton, G.R. High temperature thermodynamic properties of the chromium carbides Cr_7C_3 and Cr_3C_2 determined using a galvanic cell technique. *Metall. Trans. B* **1984**, *15*, 517–521. [CrossRef]
12. Hirota, K.; Mitani, K.; Yoshinaka, M.; Yamaguchi, O. Simultaneous synthesis and consolidation of chromium carbides (Cr_3C_2, Cr_7C_3 and $Cr_{23}C_6$) by pulsed electric-current pressure sintering. *Mater. Sci. Eng. A* **2005**, *399*, 154–160. [CrossRef]
13. Esteve, J.; Romero, J.; Gómez, M.; Lousa, A. Cathodic chromium carbide coatings for molding die applications. *Surf. Coat. Technol.* **2004**, *188*, 506–510. [CrossRef]
14. Zhang, X.; Guo, H.; Yin, F.; Fan, Y.; Zhang, Y. Interfacial microstructure and properties of diamond/Cu-xCr composites for electronic packaging applications. *Rare Met.* **2011**, *30*, 94–98. [CrossRef]
15. Hussainova, I.; Jasiuk, I.; Sardela, M.; Antonov, M. Micromechanical properties and erosive wear performance of chromium carbide based cermets. *Wear* **2009**, *267*, 152–159. [CrossRef]
16. Tian, B.; Lind, C.; Paris, O. Influence of $Cr_{23}C_6$ carbides on dynamic recrystallization in hot deformed Nimonic 80a alloys. *Met. Sci. Eng. A* **2003**, *359*, 44–51. [CrossRef]
17. Schroder, D.V.; Pribran, J.K. *An Introduction to Thermal Physics*; Addison Wesley Longman: New York, NY, USA, 1999; Volume 2008, p. 311.
18. Min, T.; Gao, Y.M.; Li, Y.F.; Yang, Y.; Li, R.T.; Xie, X.J. First-Principles Calculation Study on the Electronic Structures, Hardness and Debye Temperatures of Chromium Carbides. *Rare Met. Mater. Eng.* **2012**, *41*, 0271.
19. Hohenberg, P.; Kohn, W. Inhomogeneous electron gas. *Phys. Rev. B* **1964**, *136*, 864. [CrossRef]
20. Perdew, J.P.; Burke, K.; Ernzerhof, M. Generalized Gradient Approximation Made Simple. *Phys. Rev. Lett.* **1996**, *77*, 3865–3868. [CrossRef]
21. Fanan, S.B.; Mota, R.; Baierle, R.J.; Paiva, G.; Silva, A.J.R.D.; Fazzio, A. Stability investigation and thermal behavior of a hypothetical silicon nanotube. *J. Mol. Struct. Theochem.* **2001**, *539*, 101–106.
22. Monkhorst, H.J.; Pack, J.D. Special points for Brillouin-zone integrations. *Phys. Rev. B* **1976**, *13*, 5188. [CrossRef]
23. Jiang, D.; Zhong, S.; Xiao, W.; Liu, D.; Wu, M.; Liu, S. Structural, mechanical, electronic, and thermodynamic properties of pure tungsten metal under different pressures: A first-principles study. *Int. J. Quantum Chem.* **2020**, *120*, e26231. [CrossRef]
24. Wu, Z.J.; Zhao, E.J.; Xiang, H.P.; Hao, X.F.; Liu, X.J.; Meng, J. Crystal structures and elastic properties of superhard IrN_2 and IrN_3 from first principles. *Phys. Rev. B* **2007**, *76*, 059904. [CrossRef]
25. Šimůnek, A.; Vackář, J. Hardness of covalent and ionic crystals: First-principle calculations. *Phys. Rev. Lett.* **2006**, *96*, 085501. [CrossRef]
26. Glaser, J.; Schmitt, R.; Meyer, H.J. Neue Strukturverfeinerung und Eigenschaften von Cr_3C_2/Structure Refinement and Properties of Cr_3C_2. *Z. Nat. B* **2003**, *58*, 929–933. [CrossRef]
27. Gao, F.M. Hardness of nanocrystalline diamonds. *Phys. Rev. B* **2006**, *73*, 132104. [CrossRef]
28. Rouault, A.; Herpin, P.; Fruchart, R. Études christallographique des carbures Cr_7C_3 et Mn_7C_3. *Ann. Chim.* **1970**, *5*, 461–470.
29. Yakel, H.L. Atom distributions in tau-carbide phases: Fe and Cr distributions in $(Cr_{23-x}Fe_x)C_6$ with x = 0, 0·74, 1·70, 4·13 and 7·36. *Acta Crystallogr. B* **2010**, *43*, 230–238. [CrossRef]
30. de Wijs, G.A.; de Boer, P.K.; de Groot, R.A. Anomalous behavior of the semiconducting gap in WO_3 from first-principles calculations. *Phys. Rev. B* **1999**, *59*, 2684–2693. [CrossRef]
31. Price, D.L.; Cooper, B.R. Total energies and bonding for crystallographic structures in titanium-carbon and tungsten-carbon systems. *Phys. Rev. B* **1989**, *39*, 4945–4957. [CrossRef]
32. Xiao, B.; Xing, J.D.; Feng, J.; Zhou, C.T.; Li, Y.F.; Su, W.; Xie, Y.H. A comparative study of Cr_7C_3, Fe_3C and Fe_2B in cast iron both from ab initio calculations and experiments. *J. Phys. D Appl. Phys.* **2009**, *42*, 115415. [CrossRef]
33. Henriksson, K.O.E.; Sandberg, N.; Wallenius, J. Carbides in stainless steels: Results from ab initio investigations. *Appl. Phys. Lett.* **2008**, *93*, 191912. [CrossRef]
34. Deligoz, E.; Ciftci, Y.O.; Jochyml, P.T.; Colakoglu, K. The first principles study on PtC compound. *Mater. Chem. Phys.* **2008**, *111*, 29–33. [CrossRef]
35. Swain, M. *Structure and Properties of Ceramics*; VCH: New York, NY, USA, 1994.
36. Wang, Y.L. *Performance and Application of Functional Ceramics*; The Science Publishing Company: Beijing, China, 2003.
37. Zhou, Y. *Science of Ceramics Material*; Harbin Institute of Technology Press: Harbin, China, 1995.

38. Nam, D.; Lee, S. Effect of tempering on Microstructure, hardness, wear resistance, and fracture toughness of Cr_3C_2/steel surface composites fabricated by high-energy electron-beam irradiation. *Metall. Mater. Trans. A* **2008**, *39*, 2615–2625. [CrossRef]
39. Li, K.Y.; Yang, P.; Xue, D.F. Anisotropic hardness prediction of crystalline hard materials from the electronegativity. *Acta Mater.* **2012**, *60*, 35–42. [CrossRef]
40. Zhou, W.; Liu, L.; Li, B.; Wu, P.; Song, Q. Structural, elastic and electronic properties of intermetallics in the Pt–Sn system: A density functional investigation. *Comput. Mater. Sci.* **2009**, *46*, 921–931. [CrossRef]
41. Born, M.; Huang, K. *Dynamical Theory of Crystal Lattices*; Oxford University Press: Oxford, UK, 1954; Volume 10.
42. Nikolussi, M.; Shang, S.L.; Gressmann, T.; Leineweber, A.; Mittemeijer, E.J.; Wang, Y.; Liu, Z.K. Extreme elastic anisotropy of cementite, Fe_3C: First-principles calculations and experimental evidence. *Scr. Mater.* **2008**, *59*, 814–817. [CrossRef]
43. Jang, J.H.; Kim, I.G.; Bhadeshia, H.K.D.H. Substitutional solution of silicon in cementite: A first-principles study. *Comput. Mater. Sci.* **2009**, *44*, 1319–1326. [CrossRef]
44. Yang, Y.; Lu, H.; Yu, C.; Chen, J.M. First-principles calculations of mechanical properties of TiC and TiN. *J. Alloys Compd.* **2009**, *485*, 542–547. [CrossRef]
45. Gilman, J.J.; Roberts, B.W. Elastic Constants of TiC and TiB_2. *J. Appl. Phys.* **1961**, *32*, 1405. [CrossRef]
46. Liu, Z.L.; Chen, X.R.; Wang, Y.L. First-principles calculations of elastic properties of LiBC. *Physical B* **2006**, *381*, 139–143. [CrossRef]
47. Siwark, P.; Garbiec, D.; Rogalewicz, M. The effect of Cr_3C_2 and Ta C additives on microstructures, hardness and fracture toughness of WC-6Co tool material fabricated by spark plasma sintering. *Mater. Res.* **2017**, *20*, 780–785. [CrossRef]
48. Sin'ko, G.V.; Smirnow, N.A. Ab initio calculations of elastic constants and thermodynamic properties of bcc, fcc, and hcp Al crystals under pressure. *J. Phys. Condens. Matter* **2002**, *14*, 6989.
49. Anderson, O.L. A Simplified Method for Calculating the Debye Temperature from Elastic Constants. *J. Chem. Solids* **1963**, *24*, 909–917. [CrossRef]
50. Segall, M.D.; Lindan, P.J.D.; Probert, M.J.; Pickard, C.J.; Hasnip, P.J.; Clark, S.J.; Payne, M.C. First-principles simulation: Ideas, illustrations and the CASTEP code. *J. Phys. Condens. Matter* **2002**, *14*, 2717. [CrossRef]